Stress Corrosion Cracking Susceptibilities of Carbon Steel and its Welded Joint in High Temperature Water †

Masaru SAKAGUCHI*, Yasushi KIKUCHI and Fukuhisa MATSUDA*****

Abstract

This study was carried out in order to understand the behavior of Fan-shaped Pattern type Stress Corrosion Cracking (FSP-SCC) susceptibilities of carbon steel and its welded joints in pure water, simulating an LWR under high temperature and high pressure. The susceptibility of FSP-SCC was examined under various temperatures (373 to 573 K) and dissolved oxygen levels (0.007 to 8 ppm) as environmental factors using the slow strain-rate tensile test (SSRT).

An evaluation method for susceptibility of FSP-SCC using data obtained here, are discussed and then an optimized evaluation method is proposed. We also investigated SCC susceptibility at the welded joints..

KEY WORDS: (Stress Corrosion Cracking) (Slow Strain-Rate Tests) (Carbon Steel) (High Temperature) (High Pressure)

1. Introduction

Though carbon steels are widely used as structural materials in BWR type LWR, their SCC susceptibility has not been clarified in the BWR environment so far. [1-6]

This study was carried out using slow strain-rate tensile tests (SSRT) to study the behavior for FSP-SCC susceptibility of medium carbon steel (S45C) and its welded joints under high temperature, high pressure pure water.[7] The relationship between environmental factors of various temperatures, and dissolved oxygen contents and FSP-SCC susceptibility is summarized in the figures. Moreover SCC susceptibility at the welded joint was discussed.

2. Experimental Procedures

Specimens for the SSRT were medium carbon steel S45C (Japanese Industrial Standard, JIS), and electrode wire No65G whose chemical compositions and mechanical properties as received are listed in **Table 1**.

Table 1 Chemical composition and mechanical properties of steel tested

Material Base metal & electrode wire	Chemical composition (mass %)					Mechanical properties**			
	C	Si	Mn	P	S	Y. S (MPa)	UTS (MPa)	El. (%)	R. A. (%)
S45C*	0.45	0.17	0.78	0.027	0.017	335	705	26.6	49.6
No65G	0.03	0.54	1.19	0.009	0.014	586	648	28.0	—

* ϕ 16 mm, ** JIS Z 2201, T.P No. 4

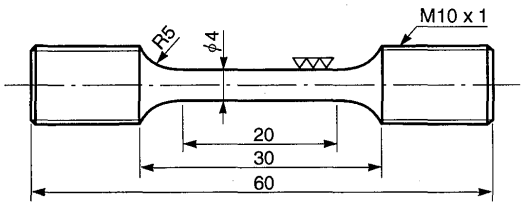

Fig. 1 Dimensions for SSRT specimen

The shape and the dimension for the SSRT specimens are shown in **figure 1**.

SSRT tests were carried out at four levels of dissolved oxygen (DO), 0.007, 0.2, 2 and 8 ppm, in water in an autoclave and six levels of temperature from 373 to 573 K (100 to 300℃) at a constant pressure of 8.3 MPa.

The strain-rate for tensile testing is a constant value of $8.3 \times 10^{-7} s^{-1}$ through the whole test.

The prescribed concentration of DO in water was controlled by supplying ion exchanged pure water from a tank. Oxygen and nitrogen were automatically introduced into the pure water in the tank to control DO. DO was always measured using a DO checking meter.

The electrical conductivity of pure water supplied using the ion exchange method is controlled to less than 1 ms/cm through the whole test. The slow strain-rate tensile test was carried out until the specimen was fractured, and

† Received on December 18, 2000

* Associate Professor, College of Industrial Technology
** Professor
*** Professor Emeritus Osaka University

Transactions of JWRI is published by Joining and Welding Research Institute of Osaka University, Ibaraki, Osaka 567-0047, Japan.

the time to failure, Tf, was measured. The elongation, λ (mm), and the reduction in area, RA (%), of the fractured specimen was measured.

The fractured specimens after SSRT were tested after descaling. The fractured surface was observed by using a SEM. The ratio of the fracture areas of fan-shaped patterns to total fractured cross section of the specimen is defined as the area of SCC fracture. Also the metallographic observation of the fractured specimens was carried out using an optical microscope.

3. Experimental Results and Discussion

Figure 2 shows the macro photographs of the fractured surface of S45C by using a SEM after testing in SSRT (518 K, 8 ppm). The areas of quasi-cleavage mode which is recognized as the SCC mode is partly observed at the edge of the fractured surface in both macro photos and are spread as fan-shaped patterns in both micro photographs, the area of which is surrounded by dimple mode fractured surface.

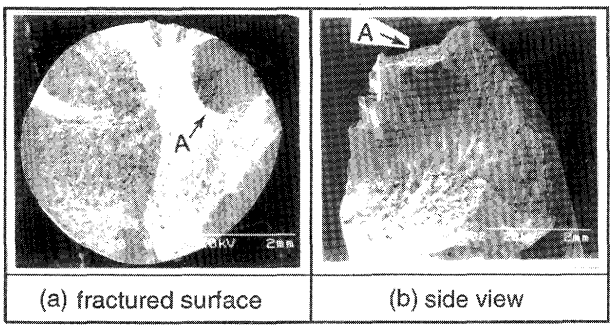

Fig. 2 Typical example of Fan-Shaped Pattern on the SEM photographs of S45C specimen tested in 8 ppm O2 water at 518 K

3.1 Influence of the testing temperature and the dissolved oxygen on the load-elongation diagram

Figure 3(a) shows schematically the load-elongation diagram of the specimens from the start of loading until fracture with different DO contents at 518 K. The results for 8 and 2 ppm of DO content in figure 3(a) shows almost the same value of elongation, Tf, RA, and FSP, about 3 mm, 49.3 - 50.7 hours, 14.2 - 17.2 % and 25.3 - 27.1 %, respectively. The large FSP fractured ratio occurred at 8 and 2 ppm of DO content.

Figure 3(b) shows the SEM photographs of the fractured surfaces for different DO contents. The FSP-SCCs are observed in 8, 2 and 0.2 ppm of DO content and are indicated using arrows in the figures. On the other hand, the result in 0.007 ppm of DO content in figure 3(a) shows elongation, c.a. 5.5 mm, about two times longer Tf, 91.1 hours, than those in 8 and 2 ppm DO content. 0 % of FSP area fraction occurred at 0.007 ppm of DO content. It was found that SCC susceptibility drastically changes due to changes in the DO content at 518 K.

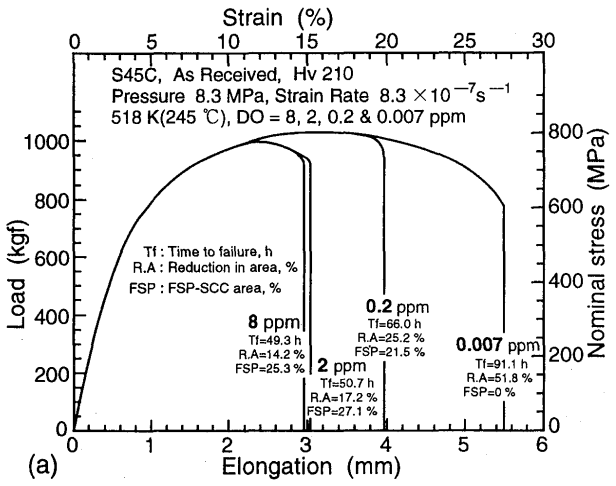

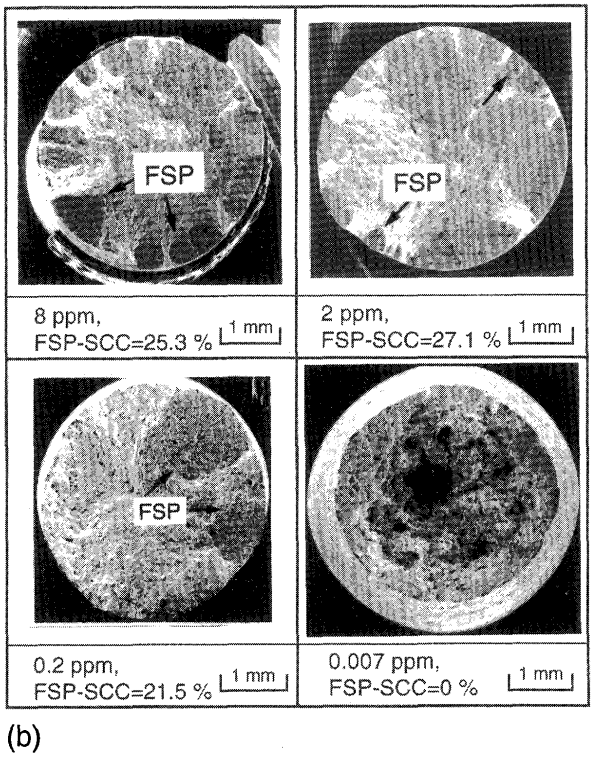

Fig. 3 S45C tested in 518 K water at various DO environments
(a) Load-Elongation diagrams
(b) Comparison among the fractured surfaces of specimens tested in 8, 2, 0.2 and 0.007 ppm O2

Figure 4 shows the time to failure Tf, for various DO contents at the tested temperatures. It is found that although there is no effect of DO contents on the Tf at

373 and 423 K, Tf decreases significantly with temperature increase in the region greater than 473 K at 8 and 2 ppm of DO content. It was considered that since the FSP fracture might occur at greater than 473 K, at which Tf decreased, there was an obvious difference in Tf at 518 K between 0.007 and 8, 2 and 0.2.

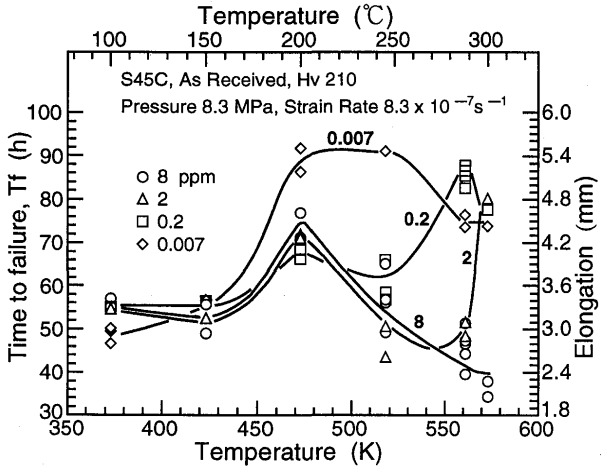

Fig. 4 Relationship between time to failure and temperature

Figure 5 shows the reduction in area, RA, for the different DO contents at the testing temperature. It is found that the difference of RA in DO between 0.007 and 8, 2, 0.2 ppm increases remarkably under no SCC condition at 518 K. From all these results, the RA values reached less than 30 % when FSP fracture occurred, while the RA reached values more than 50 % when FSP fracture didn't occur. The difference between the RA with and without occurrence of FSP fracture appeared obviously at the temperature.

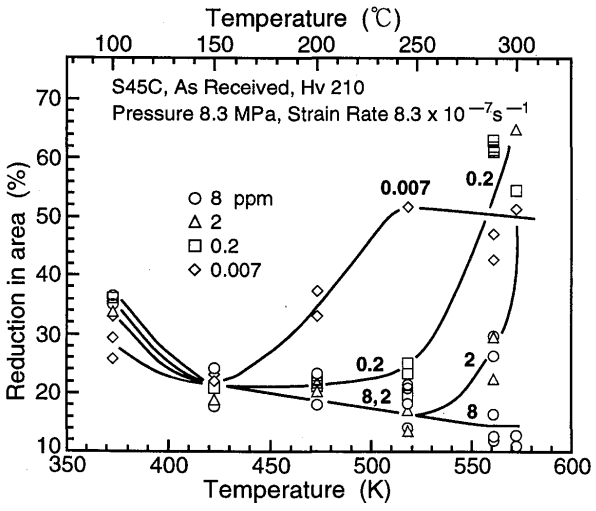

Fig. 5 Relationship between reduction in area and temperature

However, no significant difference of the RA was found with DO contents at 423 K. The RA with 0.007 ppm of DO content at temperatures greater than 473 K showed a tendency to increase.

3.2 Influence of the testing temperature and dissolved oxygen on ultimate tensile strength

Figure 6 shows the relationship between ultimate tensile strength (σ_B), which was calculated from the load-elongation diagram at each temperature, and the testing temperature. It shows that σ_B is increasing at less than 473 K and is decreasing above that temperature. Moreover, no remarkable change in σ_B is observed even with varied DO contents. When attention was paid to the temperature of 518 K at which FSP-SCC susceptibility appeared obvious, it was found that the value of σ_B varied within only a few tens of MPa, even in the FSP area fraction changing from 0 (in 0.007 ppm of DO content) to 25.3 % (in 8 ppm of DO content).

Thus, it suggested that the value of σ_B was not appropriate for the detection of the occurrence of FSP.

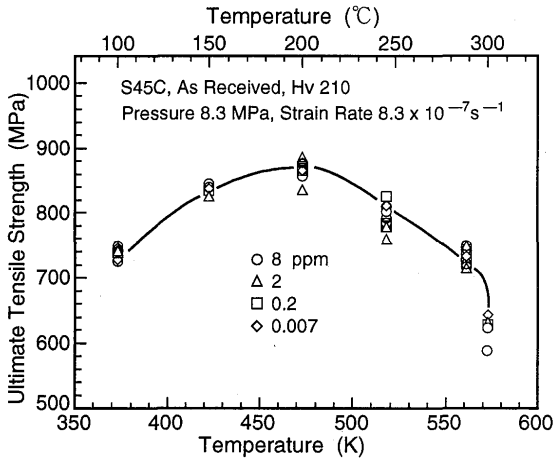

Fig. 6 Relationship between ultimate tensile strength and temperature

3.3 Discussion about the evaluation method for SCC susceptibility using SSRT

The results obtained from SSRT provide the mechanical properties, such as elongation, reduction in area, strain energy, in the load-elongation diagrams (stress-strain diagrams). These are conventionally used as the evaluation methods for SCC susceptibility by using the area ratio A_{SCC} / A_0 obtained from the area (A_{SCC}) in the load-elongation diagrams like figure 3(a) and the area (A_0) in the measured diagrams under air or oil environmental conditions. [8]

Moreover the methods using the ratio of the fracture time ratio, the value of strain when fractured, the tensile strength, the reduction in area and so on obtained from both diagrams are also used as the conventional evaluation methods for SCC susceptibility.

After we determined which evaluation methods showed the most reasonable and the best-fitted FSP-SCC fractured ratio changes, then we proposed it as the optimized evaluation method.

3.3.1 Discussion about the relationship between the FSP area fraction and testing temperature

Figure 7 shows the effect of the temperature and the DO content on the FSP area fraction of specimens. The figure shows that the evolution of FSP is not observed for all DO contents up to 423 K. Above 423 K, the evolution FSP occurs and the FSP area fraction gradually increases with temperature in 8, 2 and 0.2 ppm of DO content shown in the figure.

The maximum of FSP area fraction for 8 ppm of DO content appears at 518 to 561 K and reaches about 30 %, but with scattering. However, the FSP area fraction at 2 ppm of DO content fraction shows a maximum value at 518 K, then decreases with temperature around 518 K, and is not observed at 573 K at all.

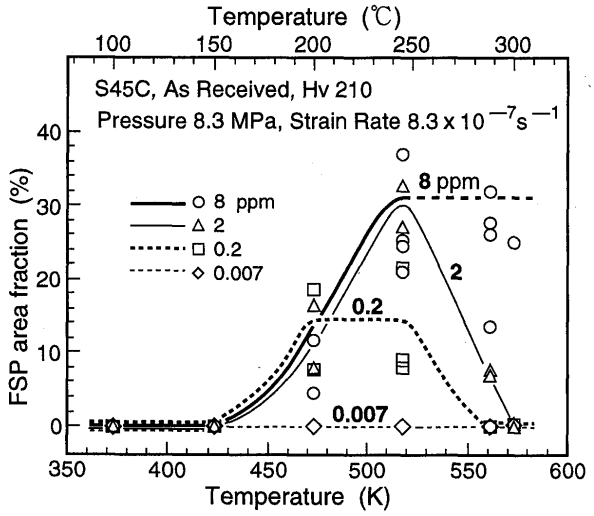

Fig. 7 Effect of temperature and oxygen on FSP area fraction

3.3.2 Relationship between the elongation ratio and SCC susceptibility

Figure 8 shows the elongation ratios, ER, for 8, 2 and 0.2 ppm of DO content and each testing temperature. These are calculated using the value of the elongation obtained in figure 4 in the DO contents based on that in 0.007 ppm of DO content with no SCC. The relationship between the elongation ratio and the temperature was that the elongation ratio decreased remarkably with increases of temperature up to 518 K as shown in the figure.

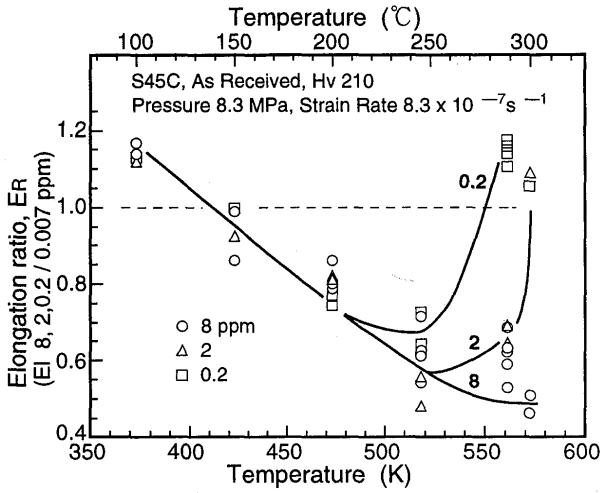

Fig. 8 Relationship between elongation ratio and temperature (ER : the ratio of the elongation in 8, 2 and 0.2 ppm O2 to that in 0.007 ppm O2)

Thus, it was found that the elongation ratio in the results also corresponded to the tendency of FSP area fraction in figure 7. Here since the broken line in figure 8 showed that the elongation ratio was 1.0, the elongation at 0.2 and 2 ppm of DO content showed the same as at 0.007 ppm with no SCC.

3.3.3 Relationship between the reduction in area ratio and SCC susceptibility

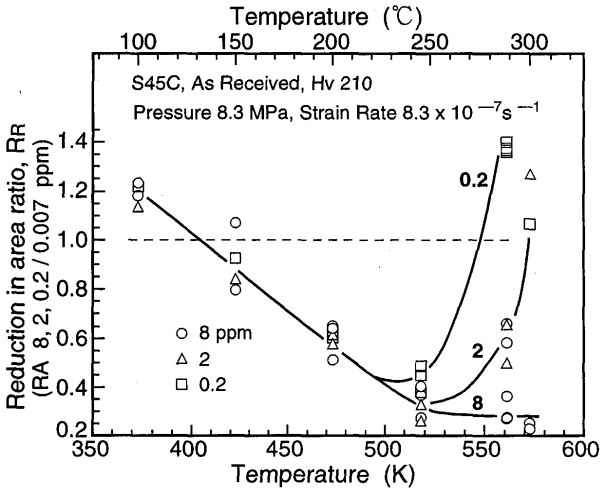

Fig. 9 Relationship between reduction in area ratio and temperature (RR: the ratio of the reduction in area in 8, 2 and 0.2 ppm O2 to that in 0.007 ppm O2)

Figure 9 shows the reductions in area ratio, RR, for 8, 2 and 0.2 ppm of DO content and each testing temperature. This is calculated as the ratio of the reduction in area shown in figure 5 for 8, 2 and 0.2 ppm of DO content to that for 0.007 ppm of DO content and no SCC.

Since the broken line in figure 9 showed that the reduction in area ratio was 1.0, the reductions in area ratio for 0.2 and 2 ppm of DO content showed the same as at 0.007 ppm with no SCC.

It was found that the tendency of the reduction in area ratio for 8, 2 and 0.2 ppm DO content was almost the same as the elongation ratio in figure 8.

Furthermore, when the tendency of the reduction in area ratio compared with the results of FSP area fraction in figure 7, it was found that the reduction in area ratio also corresponded to the FSP area fraction well.

3.3.4 Relationship between the strain energy ratio and SCC susceptibility

The strain energy, ASCC, was obtained from the area of the diagram in the stress-strain diagram measured at 518 K in shown figure 3(a) at each DO content. The ratio calculated using the strain energies for 8, 2 and 0.2 ppm DO content based, on that at 0.007 ppm, was defined as the strain energy ratio.

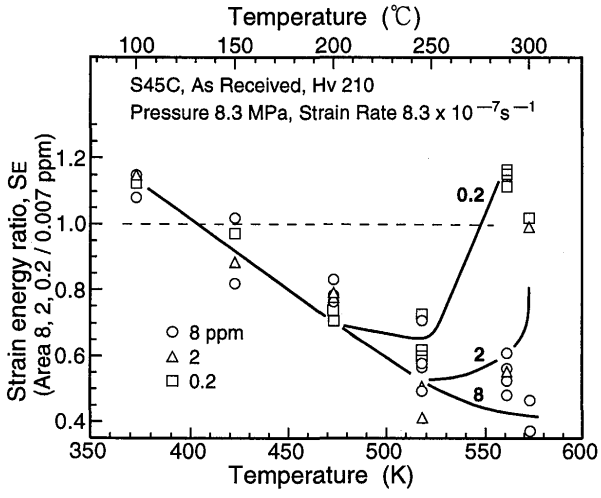

Fig. 10 Relationship between strain energy ratio and temperature (SE : the ratio of the strain energy in 8, 2 and 0.2 ppm O2 to that in 0.007 ppm O2)

Figure 10 shows the relationship between the strain energy ratio and the testing temperature. The tendency of the strain energy ratio for 8, 2 and 0.2 ppm of DO content showed almost same as those in figures 8 and 9.

3.3.5 Discussion about SCC susceptibility using SSRT

From the results of 3.3.2 to 3.3.4 described above, we consider that any of the elongation ratio (ratio of time to failure), reduction in area ratio and the strain energy ratio provides an index which can simply evaluate the FSP area fraction, namely the FSP-SCC susceptibility. The reduction area ratio showed the largest change down to 0.2 among these ratios, while the strain energy ratio and the elongation ratio showed the changes down to 0.4 and 0.5, respectively. We can judge from the above that the reduction in area ratio can best evaluate the FSP-SCC susceptibility.

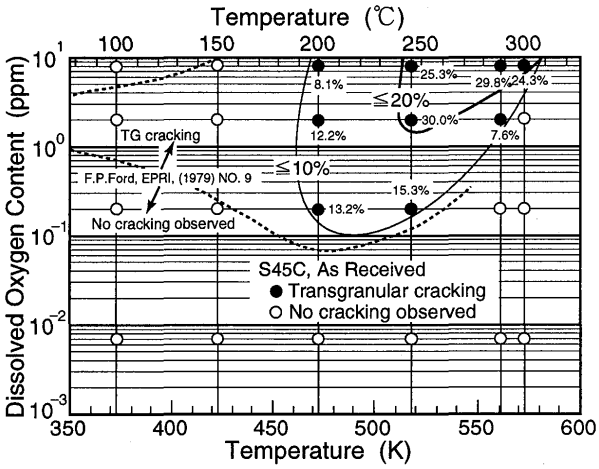

Fig. 11 Variation of the scc ratio for various oxygen/ temperature combinations 〔Figures by the symbols stand for average FSP areafraction (○) denotes no cracking observed, (●) denotes FSP observed〕

Figure 11 shows the FSP-SCC susceptibility (FSP-SCC area fraction) of S45C with testing temperature and DO. The closed circles and open circles denote FSP-SCC and no cracking observed, respectively, in the fractured surface. The indication of percentage % at the closed circle represents the average of FSP area fractions for several specimens. The solid line shows the equi-susceptible line obtained in this experiment, and the dotted line has been shown by F.P.Ford. [6]

In this experiment there was no FSP-SCC at temperatures less than 423 K (150℃) comparing with F.P.Fords result [6], and for the DO of 0.007 ppm in both steels.

3.4 SCC susceptibility at the welded joint

Welded joints made of carbon steel were prepared using S45C steel (16 mm thickness) as a base metal and No65G of 1.6 and 2.4 mm diameter as an electrode wire by GTA Welding through 12 passes (welding current :

130-140A, arc voltage:14 V, temperature between passes: c.a. 413 K). Chemical composition and mechanical properties of the electrode wire tested is listed in table 1.

Specimens including the welded joint were prepared according to the dimensions shown in figure 1. When the SCC test using welded joint specimens was done for the high SCC susceptibility condition of 518 K and 8 ppm of DO content water, both specimens failed in the base metal. The time to failure of the R specimens with welded joint decreased to about half, 22.3 and 24.6 hours, compared with that of the R specimens made of S45C.

It is considered that because of nonuniformity of hardness of the welded joint.

With specimens elongated uniformly, the local elongation was concentrated within a relatively short region at the point where the FSP was observed. It is considered that because the carbon content is low (C=0.13 %) in the weld metal and SCC susceptibility is low, FSP cannot be observed at the weld metal. The fractured surface and fractured condition are shown in **figure 12(a), (b)** and **(c)**.

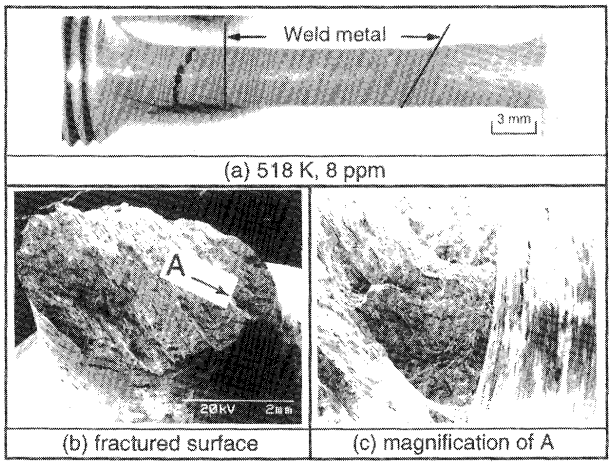

Fig. 12 The fractured surface of welded specimen tested in 8 ppm O2 water at 518 K

Figure 12(a) shows that the failure occurred at the base metal (b) shows the macro structure of the fractured surface, and (c) shows the FSP observed at the fractured surface. It was found to be difficult using this shape of specimen to study the SCC susceptibility at the weld metal, because the failure always occurred at the base metal.

Therefore in order to examine the SCC susceptibility at the certain point of welded joint, the test was done using the modified specimens (called specimen with R) which had a reduced diameter at the designated point shown in **figure 13**.

The positions of the minimum diameter of the specimen with R were (a) weld metal, (b) bond and (c) HAZ (position of 1mm apart from the bond) shown in **figure 14**.

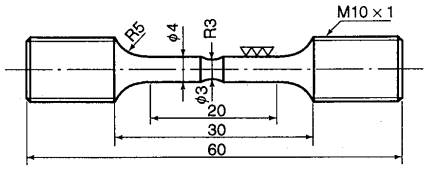

Fig. 13 Welded joint of the SSRT specimen

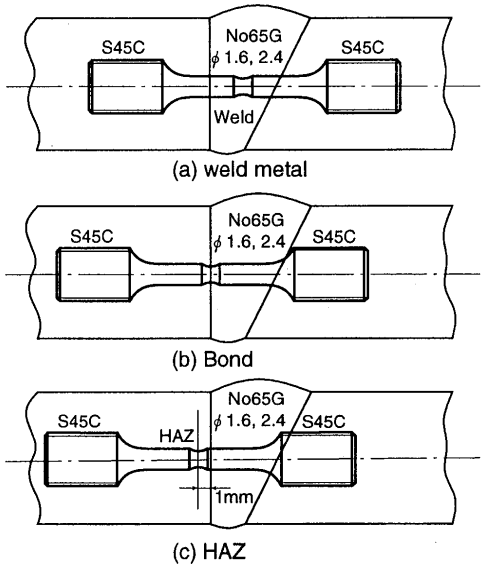

Fig. 14 SSRT specimen for different location of welded joint

3.4.1 SCC susceptibility at the position on the specimens with R

SCC tests were carried out under the selected environmental conditions of 8 ppm of DO content at both temperatures of 518 and 561 K using the specimens with R, and the relative comparisons about the possibility of occurrence of SCC and the difference of the Tf were investigated.

Figure 15 shows the Tf for the different locations of the welded joint specimens. Although any marked difference of the Tf cannot be observed in figure 15, the Tf seems to be decreasing at successively, the weld metal, the HAZ, and the bond. As the weld metal showed almost uniform hardness within a constant range, it was considered to result in a little longer Tf of the weld metal. On the other hand, the shorter Tf was considered to result from the increase in the hardness of the bond and HAZ.

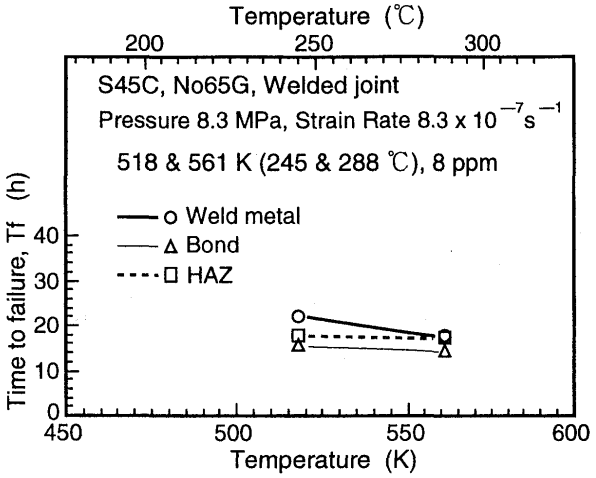

Fig. 15 Effect of different location of welded joint specimens on the time to failure

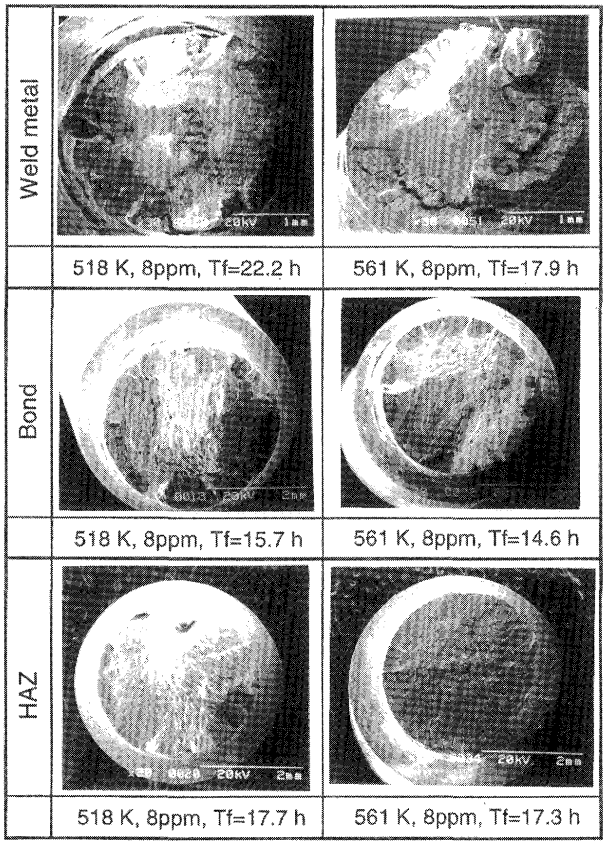

Fig. 16 Comparison among the fractured surfaces of different location of welded joint specimens tested in 8 ppm O2 water at 518 and 561 K

Figure 16 shows the SEM photographs of the fractured surfaces for 8 ppm of DO content at the temperature of 518 and 561 K. Though the open crack was observed around R in the case of the weld metal at 518 K, the fracture crossed the location of minimum diameter. Moreover only about 6.2 % of the FSP was observed at the periphery of the fracture. About 8.8 and 11.2 % of the FSP were also observed at the periphery of the fractures in the case of the bond and the HAZ, respectively.

However at the temperature of 561 K, the FSP were clearly observed, not only at the fractures in the weld metal, but also at that in the bond. It was considered from these results that the difference was not significant, because SCC susceptibility of the HAZ became almost the same as that of the weld metal and the hardening at the HAZ was not so extensive as it was in the multi-layered weld at the welded joint of S45C.

4. Conclusions

(1) When the dissolved oxygen was driven out nearly completely, to about 0.007 ppm, no FSP on the fractured surface was observed at all.

FSP-SCC didn't occur at less than 473 K for all levels of DO content, while it occurred at more than 473 K in 8, 2 and 0.2 ppm of DO content.

(2) Much difference of the tensile strength at each tested temperature at the different DO contents cannot be observed. Thus, it is considered to be difficult to evaluate FSP-SCC susceptibility using σ_B

(3) It was found that SCC susceptibility was evaluated well using the elongation ratio, the reduction in area ratio and the strain energy ratio for each DO content calculated on the basis of the elongation (at the time to failure), the reduction in area and the strain energy in the 0.007 ppm of DO content.

(4) The specimens made of S45C as the base metal containing the welded joint which had uniform diameter were fractured at locations other than the weld joint. The time to failure of the specimens was extremely shortened because of the distribution of different hardness.

(5) FSP-SCC susceptibility at the different locations of the welded joint were investigated using the specimens with R. Small FSP was observed at the base metal, the HAZ, the bond and the weld metal containing low carbon at 518 K at 8 ppm of DO content.

However, a large difference of FSP-SCC susceptibility among these locations was not observed, because these locations consisted of the multi-layered weld and no increase of hardness of HAZ was detected.

References

1) G. Kuniya et al: "Boshoku Gijutsu (in Japanese)" 32(1983), P.264.
2) G. Kuniya et al: ibid, 32(1983), P.649.
3) T. Ishihara et al: ibid, 37(1988), P.479.
4) S. Ohashi et al: "Material & Environment" 41(1992), P.224.
5) M. E. Inding: EPRI, 1979, No. 8.
6) F. P. Ford: EPRI, 1982, No. 9, NP-2406.
7) M. Sakaguchi: Ph.D. Thesis, Osaka University, Nov. 1995.
8) J. H. Payer, W. E. Berry, and W. K. Boyd: ASTM, STP-665, p.61.